

Disclosing the catalog pulsars dominating the Galactic positron flux

Luca Orusa,^{a,b} Silvia Manconi,^c Fiorenza Donato^{d,e} and Mattia Di Mauro^e

^aDepartment of Astrophysical Sciences, Princeton University,
Princeton, NJ 08544, USA

^bDepartment of Physics and Columbia Astrophysics Laboratory, Columbia University,
New York, NY 10027, USA

^cLaboratoire d'Annecy-le-Vieux de Physique Théorique (LAPTh),
CNRS, USMB, F-74940 Annecy, France

^dDipartimento di Fisica, Università di Torino,
Via P. Giuria 1, Torino, Italy

^eIstituto Nazionale di Fisica Nucleare, Sezione di Torino,
Via P. Giuria 1, 10125 Torino, Italy

E-mail: luca.orusa@princeton.edu, manconi@lapth.cnrs.fr, donato@unito.it,
mattia.dimauro@to.infn.it

Abstract. The cosmic-ray flux of positrons is measured with high precision by the space-borne particle spectrometer AMS-02. The hypothesis that pulsars and their nebulae can significantly contribute to the excess of the AMS-02 positron flux has been consolidated after the observation of a γ -ray emission at GeV and TeV energies of a few degree size around a few sources, that provide indirect evidence that electron and positron pairs are accelerated to very high energies from these sources. By modeling the emission from pulsars in the ATNF catalog, we find that combinations of positron emission from cataloged pulsars and secondary production can fit the observed AMS-02 data. Our results show that a small number of nearby, middle-aged pulsars, particularly B1055-52, Geminga (J0633+1746), and Monogem (B0656+14), dominate the positron emission, contributing up to 80% of the flux at energies above 100 GeV. From the fit to the data, we obtain a list of the most important sources for which we recommend multi-wavelength follow-up observations, particularly in the γ -ray and X-ray bands, to further constrain the injection and diffusion properties of positrons.

ArXiv ePrint: [LAPTH-051/24](https://arxiv.org/abs/2410.10951)

Contents

1	Introduction	1
2	Positrons from catalog Galactic pulsars	3
2.1	ATNF catalog	3
2.2	Positron emission model	4
2.2.1	Simulated emission parameters	5
2.3	Positron propagation to the Earth and anisotropy	6
2.4	Summary of setups and fit to AMS-02 data	8
3	Results	9
3.1	Results from fits to AMS-02 e^+ data	9
3.2	The most relevant ATNF pulsars	11
3.3	The anisotropy of the e^+ flux	16
4	Status and perspectives of multi-wavelength insights for the most relevant sources	18
4.1	The "three musketeers"	18
4.2	Other relevant sources	20
5	Conclusions	21

1 Introduction

The AMS-02 experiment has measured the cosmic positron (e^+) flux with unprecedented precision over the energy range of 0.5 to 1000 GeV [1], although the theoretical interpretation of the flux remains a topic of debate.

At low energies, below 10 GeV, the flux is likely dominated by secondary production, which occurs through interactions between cosmic rays (CRs) and the atoms in the interstellar medium (ISM) [2–6]. Current models suggest that secondary e^+ production accounts almost entirely for the flux observed by AMS-02 between 0.5 and 1 GeV and can explain between 50–70% of the measurements at 10 GeV, depending on the assumed vertical size of the diffusive halo [6]. Above 10 GeV, the presence of a e^+ excess becomes even more pronounced, and between 100 and 1000 GeV, secondary production accounts for only around 10% of the observed data. The difference between the secondary flux and the observed data cannot be explained by uncertainties in propagation effects or in the e^+ production cross sections. In particular, the latter are estimated to bring only 5 – 7% to the overall uncertainty [7]. Therefore, it is likely that primary sources of e^+ already contribute to the flux below 10 GeV.

Pulsars are considered one of the most promising Galactic sources of high-energy e^+ . These rotating neutron stars are believed to produce electron and positron pairs (e^\pm) through the spin-down mechanism, accelerating e^+ to energies that can reach up to PeV [8, 9]. Recently, γ -ray halos at TeV energies, extending a few degrees around middle-aged pulsars, have been detected by Milagro [10], HAWC [11, 12], HESS [13], and LHAASO [14, 15]. A very extended halo around Geminga has also been observed at GeV energies using Fermi-LAT data [16]. Additionally, studies of the HESS Galactic plane survey and the latest HAWC catalogs

suggest that such halos may be a common feature among Galactic pulsars [17–20]. Efforts to detect extended emissions around the Geminga pulsar using X-ray data from XMM, Chandra, NuSTAR, and SRG/*eRosita* have so far been inconclusive [21–23]. These analyses have, however, placed upper limits on the magnetic field around Geminga, suggesting it is likely below μG strength.

The observations of γ -ray halos around pulsars provide indirect evidence that e^\pm are accelerated to very high energies from these sources. In fact, very-high-energy photons are thought to be produced by CR e^\pm that escape from the pulsar wind nebula (PWN) system. After exiting the PWN and entering the ISM, the e^\pm interact with low-energy photons in the interstellar radiation field (ISRF), generating high-energy photons through inverse Compton scattering (ICS) [24, 25]. Despite this, the exact mechanism governing the transport of e^\pm in pulsar halos, and consequently the production of γ -ray emissions, remains an open question [26–30]. One of the main challenging aspects is that the size of γ -ray halos implies that the diffusion around pulsars should be a few orders of magnitude smaller than the average of the Galaxy in order to confine e^\pm more efficiently within a few tens of parsecs around the object. So far, there is no consensus and no satisfactory model that can explain the presence of inhibited diffusion around pulsars [30, 31]. For a recent review on γ -ray halos around pulsar we refer to [32].

Theoretical models that incorporate contributions from pulsars and their nebulae (pulsar in short, in what follows) have been successful in explaining the AMS-02 e^+ data. These models take into account both a small number of nearby pulsars and the cumulative emission from pulsars listed in existing catalogs [3, 33–37], as well as simulations of the Galactic pulsar population [38–41]. Several published papers agree that the cumulative distribution of Galactic pulsars can explain the entirety of the e^+ flux above 10 GeV if they convert between 1 – 10% of their spin-down power into e^\pm pairs.

The Australia Telescope National Facility Pulsar Catalog (ATNF) [42] contains thousands of Galactic pulsars, which can account for the e^+ flux detected on Earth. However, e^\pm traveling in the Galaxy are affected by propagation processes, whose main effects are energy losses and diffusion. In particular, for e^+ above 10 GeV, energy losses prevent distant sources from contributing significantly to the observed flux. Therefore, local sources—those within 1 kpc—are expected to account for the majority of the e^+ flux. Thus, local sources are the ones more likely to contribute significantly to the AMS-02 data.

In our previous paper [41], we conducted realistic simulations of the Galactic population of pulsars, calibrating their injection properties to fit AMS-02 e^+ data. Our main result was that to explain the smoothness of the data, a few nearby and middle-aged pulsars should dominate the observed flux. In this paper, we take a step forward by using the latest version of the ATNF catalog [42] to identify the most promising pulsars that can contribute to the AMS-02 e^+ flux.

We find the list of sources by considering different assumptions for the injection spectrum of e^\pm , spin-down, and particle transport models. The list of the brightest pulsars we identify could be used to determine the injection spectrum properties through multimessenger observations in X-ray and γ rays, from GeV up to TeV energies.

The paper is organized as follows: in Section 2 we report the details of the model, Section 3 we list our results, in Section 4 we show the available multi-wavelength observations of the most interesting pulsars and, finally, in Section 5 we draw our conclusions.

2 Positrons from catalog Galactic pulsars

In order to predict the contribution of a given Galactic pulsar to the e^+ flux at Earth, a number of quantities has to been defined, which we can separate into three categories, as summarized below and detailed in the following subsections.

The first set of quantities defines the characteristics of the pulsar: the distance, age and spin-down power. These are found in pulsar catalogs, and thus for observed pulsar they are fixed, while for mock pulsar populations they must be simulated [41]. The second category concerns the quantities connected to the particle emission of each pulsar, which are phenomenological parameters in our current modeling of the process. They are not directly measurable for each individual source, and their value is usually informed by the current theoretical knowledge of particle production, acceleration and emission from pulsars as well as from multi-wavelength data on specific, representative sources. Since emission parameters are not measured for each source, we simulate them following the current state-of-the-art phenomenological knowledge of these phenomena. Finally, the e^+ released from pulsars are transported in the Galaxy before reaching the Earth, and transport parameters connected to the propagation in the ISM, including diffusion and energy losses, are needed to define the modeling of this part of e^+ journey. For this category, we assume equal transport parameters for all sources, thus assuming the properties of the ISM to be on average similar for pulsars located in the Galactic disk.

In what follows, we identify and detail our benchmark setup for the modeling of e^+ emission and propagation and the required parameters for each of these categories, together with three main variations, designed to explore the consequences of the uncertainty in the emission and propagation modeling on our results. Our main setups are summarized in Section 2.4.

2.1 ATNF catalog

The sample of pulsars considered in this work is taken from the ATNF pulsar catalog [42], version 2.1.1 ¹, which lists the observed rotation-powered pulsars, including those detected only at high energies. Within this version of the ATNF catalog, the distance to each pulsar is estimated using the most updated electron-density model [43]. However, the choice of electron-density model introduces unavoidably biases in the distance estimates, which can significantly impact the computation of the e^+ flux. The model in [43] could lead to artificial small distances of some pulsars, as for instance the distance to the source B1055-52, which can vary between 714 pc and 93 pc, depending on the Galactic free-electron density model used [43, 44].

Sources are selected by excluding all the millisecond pulsars, namely cutting off rotation periods $P_0 < 0.01$ s. The emission coming from these sources would require a different model with respect to what implemented in this work. Furthermore, it has been shown to be negligible through an analysis realized with simulations of the millisecond pulsar population [45].

After these selection cuts, a sample of 2261 pulsar is retained with a measured value of distance, age and spin-down power. We recognize in the sample notable sources such as Geminga and Monogem (J0633+1746 and B0656+14), which have been considered to be main candidates to contribute significantly to the e^+ flux at hundreds of GeV. Among the

¹<http://www.atnf.csiro.au/research/pulsar/psrcat>

selected sample, 181 pulsars have distances estimated to be less than 1 kpc, and 390 have ages between 50 kyr and 10^3 kyr. The number of pulsars having spin-down power exceeding $\dot{E} > 10^{34}$ erg/s, so with energetics comparable to the one of Geminga and Monogem, is 287.

2.2 Positron emission model

Pulsars are rotating neutron stars with a strong surface magnetic field, and magnetic dipole radiation is believed to provide a good description for their observed loss of rotational energy [8, 9]. We consider that both e^\pm are continuously accelerated and injected in the ISM at a rate that follows the pulsar spin-down energy. This scenario is indeed required to generate the TeV photons detected by Milagro and HAWC for Geminga and Monogem pulsar halos [16, 30, 46, 47]. We remind here the main aspects for the emission model of e^\pm from pulsars. The formalism is more extensively presented in [16, 41], to which we refer for further details.

The injection spectrum $Q(E, t)$ of e^\pm in the ISM at energy E and time t is described as a broken power law [11, 16]:

$$Q(E, t) = L(t)e^{-E/E_c} \times \begin{cases} (E/E_b)^{-\gamma_L} & E < E_b \\ (E/E_b)^{-\gamma_H} & E \geq E_b, \end{cases} \quad (2.1)$$

where the cut-off energy E_c is fixed at 10^3 TeV, E_b is the break at energies of the order of hundreds of GeV, and γ_L , γ_H are the slopes below and above the break energy. The broken power-law model is compatible with multi-wavelength observations of PWNe, although there are large uncertainties on specific values of these parameters for each source [48]. The magnetic dipole braking $L(t)$ is described by the function:

$$L(t) = \frac{L_0}{\left(1 + \frac{t}{\tau_0}\right)^{\frac{n+1}{n-1}}} \quad (2.2)$$

where τ_0 is the characteristic time scale and n defines the magnetic braking index. The total energy emitted by the source only into e^+ is given by:

$$E_{tot} = \eta W_0 = \int_0^T dt \int_{E_1}^\infty dE E Q(E, t) \quad (2.3)$$

through which we obtain the value of L_0 , fixing $E_1=0.1$ GeV [49, 50]. The parameter η encodes the efficiency of conversion of the spin-down energy into e^+ (which is half of the efficiency of conversion into e^\pm). Changing the value of E_1 affects the normalization of the total spectrum, which in turn impacts the efficiency η of individual sources. For the injection spectrum parameters used in this work, as listed in Table 1, setting E_1 to the e^+ mass can result in a maximum renormalization of the flux obtained with $E_1 = 0.1$ GeV by a factor of 0.65. This occurs for $\gamma_L = 2$ and $\gamma_F = 2.8$, which represents the specific parameter set that maximizes the effect of lowering the E_1 value. Choosing, on the other hand, values of E_1 larger than 0.1 GeV would lead to a flux renormalization greater than 1, thereby requiring lower efficiencies. W_0 is the initial rotational energy of a pulsar and can be computed from the pulsar age T , the spin-down luminosity \dot{E} and the decay time τ_0 :

$$W_0 = \tau_0 \dot{E} \left(1 + \frac{T}{\tau_0}\right)^{\frac{n+1}{n-1}}. \quad (2.4)$$

Here $\dot{E} = dE_{\text{rot}}/dt$ is the rate at which the pulsar rotational kinetic energy is dissipated and is called spin-down luminosity. The *actual* age T and the *observed* age t_{obs} are related by the source distance d by $T = t_{\text{obs}} + d/c$. It is possible to derive the value of τ_0 from the initial rotation period of the pulsar P_0 and its first derivative, as:

$$\tau_0 = \frac{P_0}{(n-1)\dot{P}_0}. \quad (2.5)$$

Assuming a small deviation from the dipole nature of the magnetic field B of the pulsar, \dot{P}_0 may be obtained from $P^{n-2}\dot{P} = ak(B \sin \alpha)^2$ [51], where the angle $\alpha > 0$ describes the inclination of the magnetic dipole with respect to the rotation axis, and a and k are constants that depend on the canonical characteristics of neutron stars (see [52] for details).

2.2.1 Simulated emission parameters

While the age and spin-down power are characteristics available for pulsars identified in catalogs, it is not possible to derive the value of τ_0 , the spectral indexes and the conversion efficiency directly from the current measurements, and assumptions about other quantities involved, e.g. in the calculation of τ_0 , are thus necessary. To complement the emission parameters not directly listed in pulsar catalog for each source, we proceed as follows.

As for the typical decay time τ_0 , we either assume a unique value of $\tau_0 = 10$ kyr for all the sources, a reference usually adopted in literature (see e.g. [11, 16]), or draw a distribution obtained from the simulation of artificial values of P_0 , n , B , and α for each source. In the latter setup, in order to assign to each pulsar a τ_0 value, we extended the functions implemented in the Python module `gammapy.astro.population` [53, 54] to sample the values of P_0 , B , n and α from the distributions provided in [52] (CB20). From these quantities, we extract the value of τ_0 accordingly for each source. In this way, a distribution of τ_0 starting from realistic distributions of the other quantities is obtained. If not stated differently, this represents the benchmark setup in our computations.

Since the spectrum of accelerated particles is uncertain, and may vary significantly for each source [33, 55], we sample γ_L from uniform distributions within $[1.0 - 2.0]$, γ_H within $[2.0 - 2.8]$ and E_b within $[300 - 600]$ GeV. Finally, the value of η for each source is sampled from a uniform distribution in the range $[0.01 - 0.1]$.

Unless differently stated, we will consider all the pairs produced by sources with ages above 50 kyr, since e^\pm accelerated to TeV energies in the termination shock are believed to be confined in the nebula or in the supernova remnant (SNR) until the merger of this system with the ISM, estimated to occur tens of kyr after the pulsar formation [56]. We thus leave out young sources for which the e^\pm pairs might still be confined in the parent remnant. However, this effective treatment does not account for possible spectral or time-dependent modifications of the released particles. To understand the consequences of this assumption on the interpretation of the e^+ flux at Earth, we also test the hypothesis that only the e^\pm produced after the pulsar escapes from the SNR contribute to the flux at the Earth. Following [39, 41], we define t_{BS} as the time at which the source leaves the parent SNR due to its proper motion and eventually forms a bow-shock nebula. The escape time of the pulsar from the remnant is described by:

$$t_{BS} \simeq 56 \left(\frac{E_{SN}}{10^{51} \text{erg}} \right)^{\frac{1}{3}} \left(\frac{n_0}{3 \text{ cm}^{-3}} \right)^{-\frac{1}{3}} \left(\frac{v_k}{280 \text{ km/s}} \right)^{-\frac{5}{3}} \text{ kyr} \quad (2.6)$$

where n_0 is the ISM density around the SNR taken to be 3 cm^{-3} , $E_{SN} = 10^{51} \text{ erg}$ is the energy emitted by the SN explosion and v_k is the birth velocity of the pulsar. The formalism is reported in [57], to which we refer for further details. The parameter values are taken from [39] to ensure consistency with the analysis framework used in that study. To test the scenario described by Eq. (2.6), for each source its birth-kick velocity is simulated, adopting its distribution as reported in [58] (FK06VB) and implemented in `gammapy.astro.population` [53, 54], which is the sum of two Gaussians (see their Eq. 7) for each of the three velocity components.

2.3 Positron propagation to the Earth and anisotropy

Once charged particles are injected into the Galaxy, they can propagate and eventually reach the Earth. Here, we briefly outline our treatment of Galactic propagation of e^\pm and refer the reader to [40, 41, 59, 60] for further details. The number density per unit time and volume, $N_e(E, \mathbf{r}, t)$, of e^\pm at observed energy E , position \mathbf{r} in the Galaxy, and time t , which is the solution to the propagation equation considering only an homogeneous diffusion and energy losses, is given by [16]:

$$N_e(E, \mathbf{r}, t) = \int_0^t dt' \frac{b(E_s)}{b(E)} \frac{1}{(\pi \lambda^2(t', t, E))^{\frac{3}{2}}} \exp\left(-\frac{|\mathbf{r} - \mathbf{r}_s|^2}{\lambda^2(t', t, E)}\right) Q(E_s, t') \quad (2.7)$$

where the integration over t' accounts for the source releasing e^\pm continuously in time. The energy E_s is the initial energy of e^\pm that cool down to E in a loss time $\Delta\tau$:

$$\Delta\tau \equiv \int_E^{E_s} \frac{dE'}{b(E')} = t - t_{obs}. \quad (2.8)$$

The $b(E)$ term is the energy loss rate, \mathbf{r}_s indicates the source position, and λ is the typical propagation length defined as:

$$\lambda^2 = \lambda^2(E, E_s) \equiv 4 \int_E^{E_s} dE' \frac{D(E')}{b(E')} \quad (2.9)$$

where $D(E)$ is the diffusion coefficient taken as a double broke power-law in energy [6]. The e^\pm energy losses include ICS off the ISRF and the synchrotron emission on the Galactic magnetic field. The flux of e^\pm at the Earth for a source of age T and distance $d = |\mathbf{r}_\odot - \mathbf{r}_s|$ is given by:

$$\Phi_{e^\pm}(E) = \frac{c}{4\pi} N_e(E, \mathbf{r} = \mathbf{r}_\odot, t = T). \quad (2.10)$$

The propagation parameters are fixed to the ones derived in [6] from a fit to the latest data measured by the AMS-02 experiment, particularly the absolute fluxes of protons, He, C, O, N, B/C, Be/C, and Li/C after 7 years of data collection, from 2011 to 2018 [61], complemented with proton and helium data from Voyager [62]. Specifically, we consider their benchmark model `Conv` dv_c/dz , with the value of L fixed at 4 kpc (see Table 2 of [6] for the values of the parameters of this model). We note that, however, the parameter L is not relevant in this study since we implement solutions without boundaries both in the radial and the vertical directions reported in Eq. 2.7. The infinite halo approximation has been widely used to compute the flux from single sources located in the Galactic plane in [36, 40, 63]. We verified that our conclusions remain unchanged when adopting a more refined approach, incorporating

the halo size $L = 4$ kpc using the image charge method described in [64], which modifies the infinite halo solution reported in our Eq. 2.7 (see Eq. 2 of their paper). By evaluating 100 realizations of one of our setups, later referred to as the τ_0 **distribution** model (see Sec. 2.4), we found that the mean deviation between the total e^+ flux from pulsars obtained with the boundary condition and the infinite halo approximation is less than 1% at $E = 10$ GeV and decreases further at higher energies.

Energy losses are computed on the interstellar photon populations at different wavelengths following the default GALPROP model, which is consistent with more recent estimates in the few kpc around the Earth [65], taking into account Klein-Nishina corrections for ICS, and setting the Galactic magnetic field with an intensity of $B = 3 \mu\text{G}$.

We also test how the results change considering a two-zone diffusive zone around each pulsar. Recent results [11, 16, 66] suggest that the diffusion coefficient around Geminga, Monogem, and PSR J0622+3749 is $\sim 10^{26} \text{ cm}^2/\text{s}$ at 1 GeV, *i.e.* about two orders of magnitude smaller than the value derived for the entire Galaxy through a fit to AMS-02 CR nuclei data [67–69], although different interpretations have been proposed [30]. A phenomenological description for this discrepancy proposes a two-zone diffusion model, where the region of low diffusion is contained around the source and delimited by an empirical radius r_b [70–72]. We stress here that our main purpose is to derive the consequences of the presence of such inefficient diffusion zones around Galactic pulsars using such a phenomenological description, while no attempt is made to provide a detailed theoretical interpretation of this phenomenon (see for different possible explanations [30, 73–78]). When using a two-zone diffusion scenario, we implement the solutions to the propagation equation reported in Ref. [16, 71]. According to the results of [11, 16, 18, 79], the radius r_b of the low-diffusion zones is at least $r_b > 30$ pc. We will adopt a value of $r_b=60$ pc (see e.g. [40] for a discussion about the variation of r_b).

Finally, we estimate the e^+ dipole anisotropy that arises from each realization of Galactic pulsars. We note that to properly model a possible anisotropy, a complete spherical harmonic decomposition of the flux should be employed. In such a framework, the flux intensity can be expressed as a sum of multipoles depending on the direction: $I(\theta, \phi) = \sum A_{lm} Y_l^m(\theta, \phi)$, where $Y_l^m(\theta, \phi)$ are the spherical harmonics and A_{lm} are the constant coefficients. However, under the assumption that one or a few nearby sources dominate, the dipole term will likely provide the main contribution to the multipole expansion. We here follow the formalism originally derived by [80] and summarized in [35, 81] in order to compute the total e^+ anisotropy resulting from a collection of sources with specific positions in the sky, as provided in the ATNF catalog. We will end up with a prediction of the dipole anisotropy as a function of energy.

The analysis is based on the standard, homogeneous diffusion model of CR propagation, without accounting for additional uncertainties that may arise from more refined propagation models. This standard model is calibrated to reproduce observations of diffuse CR nuclei fluxes but does not include localized effects near Earth. Such effects could be especially relevant for e^+ and e^- fluxes, given their relatively shorter diffusion-loss length with respect to stable CR nuclei. In particular, this approach overlooks the influence of nearby structures like the Local Bubble [82], superbubbles, and the orientation of the regular Galactic magnetic field, which can induce anisotropic diffusion. Models of the Galactic magnetic field, such as those described in [83–85], suggest that anisotropic diffusion can significantly alter the contribution of individual sources to the observed flux at Earth. While these considerations are beyond the scope of the current study, they underscore the interest to account for such effects, characterized by large uncertainties, in future analyses to achieve a more complete

Pulsar property	Simulated quantity	Benchmark	Variations
Spin-down	τ_0	Distribution from [52]	10 kyr
e^\pm injection	γ_L	Uniform [1.0-2.0]	-
	γ_H	Uniform [2.0-2.8]	-
	E_b	Uniform [300-600] GeV	-
	η	Uniform [0.01-0.1]	-
Kick velocity	v_k	-	FK06VB [58]

Table 1: Summary of the emission parameters simulated for each catalog pulsar. The simulated quantities (first two columns), the distributions adopted in their simulation, together with the boundary of their validity range, for our benchmark case (third column), as well as the tested variations (last column) are reported. See Section 2.4 for details.

understanding of CR propagation and e^\pm fluxes.

2.4 Summary of setups and fit to AMS-02 data

As explained in the previous Sections, in order to compute the e^\pm flux at the Earth for each known catalog pulsar, the source term $Q(E, t)$ (see eq. (2.1)) needs to be specified. This includes quantities that are not measured and provided directly in catalogs, for which we set up simulations, while distance, age and \dot{E} are taken directly from the catalog. Specifically, in our benchmark setup the quantities that we simulate are: τ_0 , γ_L , γ_H , E_b and η . For an alternative setup, we also simulate the birth-kick velocity v_k . A summary of these simulated quantities, together with the distribution adopted to simulate each value is illustrated in Table 1.

We recap and label here the different setups investigated using AMS-02 data in what follows. For each realization we compute the e^\pm flux from every source in the catalog sample defined in Section 2.1.

τ_0 distribution. This is our benchmark setup. The τ_0 values for each source are simulated following CB20 [52]. η , γ_L , γ_H and E_b are extracted from uniform distributions, while the propagation in the Galaxy is modeled using the transport parameters corresponding to the model `Conv` dv_c/dz from [6].

τ_0 fixed. Same as the benchmark setup, but with the value of τ_0 fixed to 10 kyr for each source.

Delayed injection. Same as the benchmark setup, but considering only the e^\pm emitted after the escaping of pulsars from the SNR. An additional parameter, the birth kick velocity, is simulated for each pulsar, and values are sampled adopting the distribution FK06VB reported in [58].

Two zone propagation Same as the benchmark setup, but considering the presence of a slow diffusion halo around each pulsar with size $r_b = 60$ pc and a diffusion coefficient $D(E) = 10^{26} \text{ cm}^2/\text{s}$ for $r < r_b$.

Depending on the setup, a number ranging between 1000 to 3000 realization N_{rea} of the e^+ emission parameters is performed, as some models adapt more easily to the data than others. The e^+ flux from each Galactic pulsar is computed accordingly. Each realization consists of the sum of the contribution of all the Galactic pulsar considered, and is fitted to AMS-02 e^+ data [1] above 10 GeV, to minimize the impact of solar modulation and other low-energy effects [86]. In each fit, a secondary component coming from cosmic ray fragmentation in the ISM is added, consistently with the implemented propagation model, as derived in [6]. Both the total contributions of pulsars and the secondary component are multiplied by normalization factors, A_P and A_S respectively, whose values are determined for each simulation through the fitting procedure. The secondary component's normalization factor, A_S , is allowed to vary between 0.01 and 2. The broad range considered here is justified by the fact that secondary production is significantly influenced by the diffusion coefficient associated with various sizes of the diffusive halo, denoted as L . On the other hand, in the energy range under examination (10 GeV–1 TeV), where energy losses dominate, the contribution from primary sources does not exhibit this pronounced dependency on the diffusion coefficient, and its sensitivity to changes in L is quite weak. Adjusting the normalization of the secondary production provides an effective means of exploring potential values for L and, consequently, the diffusion coefficient, without the need for recalculating the primary flux.

Similarly to A_S , the total flux from all pulsars is adjusted by an overall normalization factor, A_P . Both are determined for each realization through the fitting procedure.

Predictions are corrected for solar modulation using the force field approximation, with the Fisk potential ϕ free to vary between 0.4 and 1.2 GV. The comparison with AMS-02 e^+ data is performed via standard χ^2 minimization. We disregard systematic error correlations in the AMS-02 data due to the lack of information provided by the Collaboration [1].

For each setup, the realizations are filtered using as criteria the quality of the fit of the cumulative emission from all the Galactic pulsars and the secondaries to AMS-02 data. The contribution from each individual source is stored to identify a possible set of sources contributing significantly to the e^+ flux, and their underlying properties.

3 Results

The aim of this paper is to probe if the e^+ flux measured by the AMS-02 experiment [1] can be explained merely by a secondary component and by the emission from catalogued pulsars. In those models where this occurs, we investigate a hierarchy among the most relevant emitters.

3.1 Results from fits to AMS-02 e^+ data

As a first result, we show in Table 2 the number of realizations that provide a good fit to AMS-02 data, having $\chi^2/d.o.f. = \chi_{red}^2 < 1.5$, and for each setup (see Sect. 2.4). First of all, we note that each framework finds realizations which fit well the AMS-02 data. Notwithstanding that the statistical variation of their number does not bring a deep physical meaning, the τ_0 **fixed** model fits nicely the data most of the times. A fixed τ_0 for all the pulsars, clearly unrealistic, intrinsically predicts similar contributions among the sources (see Eq. (2.4)). It is then more likely to have a smoother total contribution to the e^+ flux than in cases in which few very bright sources can be switched on, and thus an easier fit to the pretty unstructured data. This also means that the other simulated parameters do not significantly impact the e^+ production, leading to realizations that are quite similar to each other. At variance, the τ_0

	N_{rea}	$\chi_{red}^2 < 1.5$	A_S	A_P	$N_{10^{-4}}$
τ_0 distribution	3000	72	1.3	0.6	3.6
τ_0 fixed	1000	768	1.0	0.8	6.7
Delayed injection	2000	194	1.2	4.6	5.3
Two zone	3000	159	1.5	0.2	3.1

Table 2: In order: model considered; number of total realizations N_{rea} tested for each model; number of realizations that produce a χ_{red}^2 smaller than 1.5 in the fit to AMS-02 data [1]; average normalization of the secondary flux (A_S) and of the total pulsar contribution (A_P) obtained for the simulations that produce a $\chi_{red}^2 < 1.5$; average number of sources satisfying the 10^{-4} criterion (see the text for details) for the simulations that produce a $\chi_{red}^2 < 1.5$.

distribution modeling can give rise to potentially extremely bright sources during the early stages of their life. The resulting total e^+ flux from all the pulsars can thus have peculiar structures, which harshly fit the data. Regarding the allowed overall normalization A_P of the pulsar primary flux for **τ_0 fixed** and **τ_0 distribution**, we generally find values slightly smaller than one, compatible with previous works [38, 41, 87].

In the **Delayed injection** setup, only the e^+ produced after the pulsar has left the remnant are considered. This approach reduces the influence of extremely bright sources, as most e^+ are produced in the early stages of the pulsar’s lifetime, i.e. $\lesssim 50$ kyr. Consequently, the total flux has not strong peaks and follows generally a smooth trend. However, the fit requires efficiencies between 5 and 46% - implied in the value of A_P - since the model does not account for the significant amount of e^+ produced at the beginning of the pulsar’s lifetime. Efficiencies close to 50%, although compatible with previous estimates obtained with the same model [39, 41], are in tension with the values obtained from the analysis of γ -ray halos around pulsars [16, 30, 32, 79], assuming a slow diffusion around this sources. They result although to be compatible with the ballistic scenario proposed in [30], which does not invoke a suppressed diffusion around pulsars. Changing the value of E_1 in the normalization of the spectrum from 0.1 to the e^+ mass can, for some specific set of parameters in the injection spectrum (γ_L close to 2 and $\eta > 33\%$ of the single pulsars), lead to unphysical values of η for individual sources. However, this occurs only in a small region of the parameter space. The average value of η required remains below 50%. In all the three models, good fits come with a normalization A_S of secondary e^+ close to one, which marks a significant improvement compared to previous predictions [4, 41]. We ascribe this result to the new computation of the secondary source term, in which the e^+ production cross sections have been adapted to a bunch of accelerator data [7].

For the **Two zone**, we obtained results similar to **τ_0 distribution**, although with a higher A_S . This outcome can be attributed to the physics of two-zone diffusion model, which tends to trap e^+ longer around the pulsar bubble, potentially preventing older sources from contributing to the 10 – 40 GeV range. However, the goodness of the fits is somehow dimmed by the necessity of some up-scaling of the secondary flux ($A_S = 1.5$ on average) and a severe downgrading of the overall pulsar contribution ($A_P = 0.2$ on average).

In Figure 1, we display the e^+ flux for four illustrative realizations with $\chi_{red}^2 < 1$, across different setups. The plots include contributions from each catalogued pulsar, the secondary emission, and their sum alongside the AMS-02 data. Overall, the contributions from pulsars become significant above 10 – 20 GeV, dominate in the 40 – 1000 GeV range,

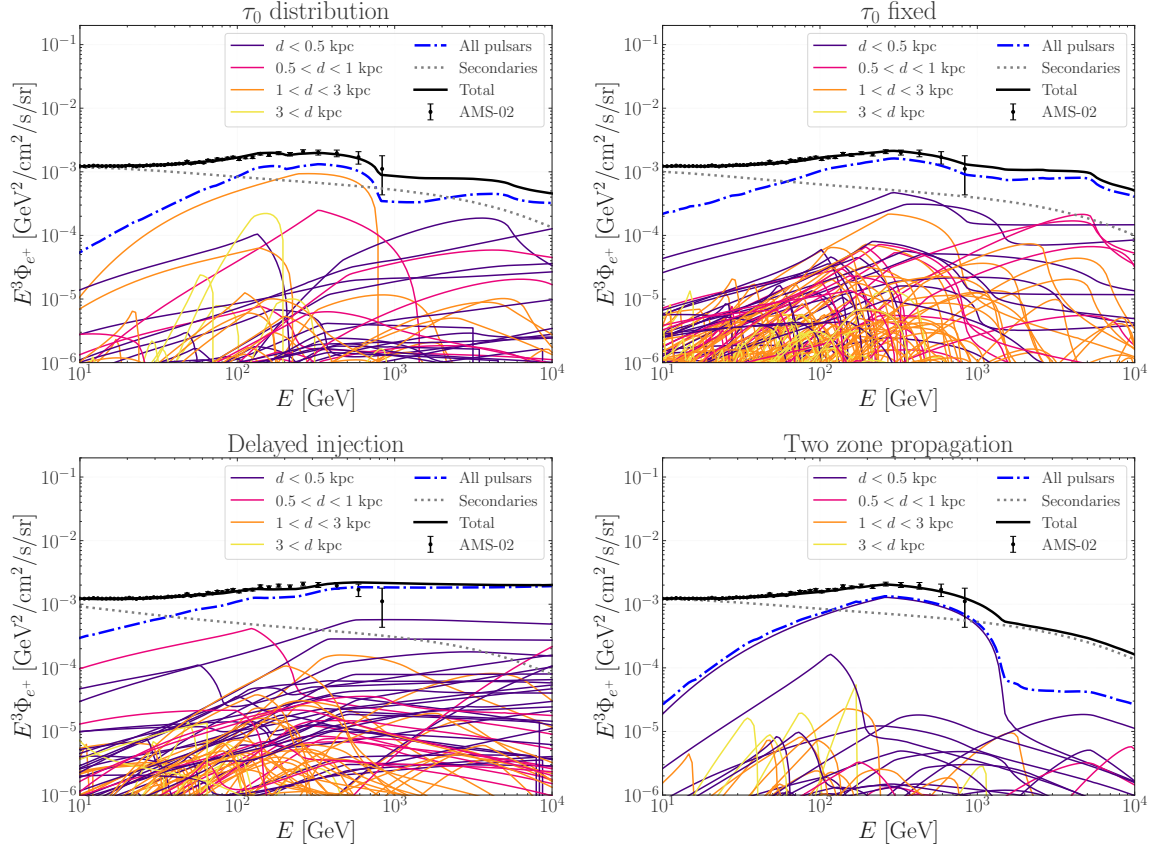


Figure 1: Comparison between the AMS-02 e^+ flux data [1] (black points) and the flux from secondary production (grey dashed line) and pulsars (blue dashed line) for four realizations of the different models that we tested with $\chi^2_{\text{red}} < 1$. The contributions from each source, reported with different colors depending on their distance from the Earth, are shown.

and show variegated features at unconstrained energies above 1 TeV, depending on the specific realization. The most intense contributions come from sources located within 1 kpc. However, statistical variations can occasionally promote more distant sources to produce a large e^+ flux, as shown in the upper left panel of Fig. 1.

3.2 The most relevant ATNF pulsars

One of the main goals of this paper is to identify the sources that most significantly contribute to the e^+ flux and shape its profile, based on different models of pulsar evolution, and e^\pm emission and diffusion. This will help prioritize the sources and provide indications for multi-messenger observations, in order to better understand their injection physics.

Our initial goal is to verify whether a small number of bright sources are sufficient to account for the majority of the e^+ excess, as found in our previous work based on full simulations of the Galactic pulsar population [41]. We show in Fig. 2 (left panel) the average flux percentage produced by the top 10 brightest sources, in each realization that fits the data, along with the 68% containment band for the different models, and relative to the

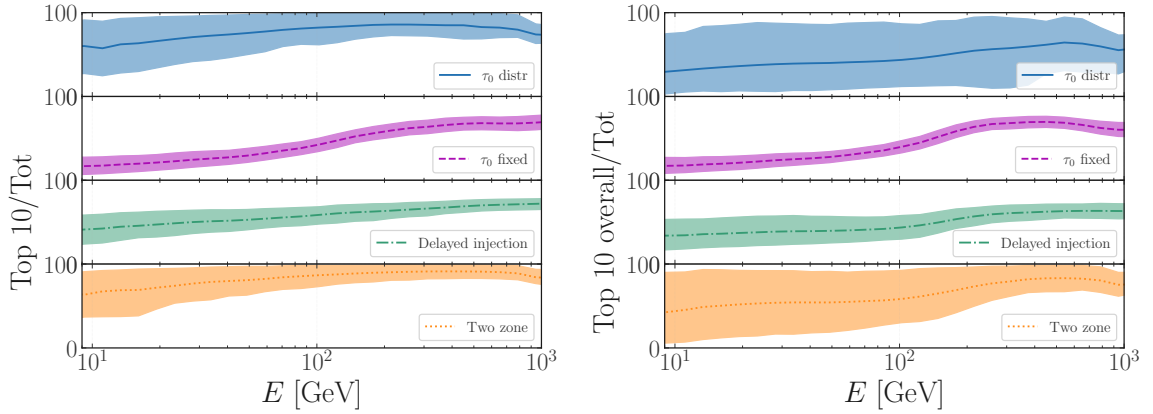


Figure 2: Left panel: the average flux percentage produced by the top 10 brightest sources in each realization that fits the data, along with the 68% containment band, for the different models, relative to the total flux produced by all pulsars. Right panel: same as left panel, but considering this time the top 10 brightest sources among the different models listed in column 5 of Table 3.

total flux produced by all pulsars. Focusing on energies above 100 GeV, the top 10 pulsars contribute nearly 80% of the total flux for all models. In the **τ_0 distribution** and **Two zone** cases, which are more sensitive to the dominance of a few sources, the 10 brightest sources explain almost the total of the e^+ produced in the Galaxy. Meanwhile, **τ_0 fixed** and **Delayed injection** lower edge of the bands show a minimum contribution around 50%.

In Fig. 3 the average values of the fluxes of the top 10 brightest pulsars are shown for each realization that fits the data, alongside the secondary flux, the contribution from the other pulsars, and their sum. We also report the 68% containment band. The role of the 10 brightest pulsars in shaping the high-energy total flux is evident everywhere. Also in the **τ_0 fixed** case, where very few dominant sources are not expected, the global trend is influenced by the top 10 pulsars.

We then apply a threshold criterion to determine which sources are responsible for the most significant contribution of pulsars to the e^+ emission, in realizations that fit the data. The rule - referred to as the 10^{-4} criterion - is for a source to have a flux at an energy E such that $E^3\Phi(E) > 10^{-4} \text{ GeV}^2/\text{cm}^2/\text{s}/\text{sr}$ for at least one energy value between 10 GeV and 1 TeV. The average number of sources satisfying this criterion across the different setups is reported in Column 6 of Table 2. The number of powerful sources according to this criterion is low, between 3.1 and 6.7. As expected, **τ_0 fixed** is the model with the highest number of contributing sources, justified by the adoption of the same τ_0 .

We now investigate possible correlations and patterns in the injection parameters of the brightest sources, considering only the realizations that successfully fit the data. Fig. 4 shows the distributions of γ_L and γ_H (see Eq. (2.1)) for the different models, obtained for the bright sources able to satisfy the 10^{-4} criterion. A clear trend emerges, favoring high values of γ_H , a requirement previously highlighted in [39]. This differs from what is typically inferred from the emission of well-studied PWNe, such as the Crab Nebula [48, 88–93], which favors values of $\gamma_H \sim 2.3 - 2.5$. This discrepancy may indicate that the particle population released by these objects undergoes significant energy losses before escaping the vicinity of the source, thereby softening the spectrum. On the other hand, we do not observe a clear trend in the

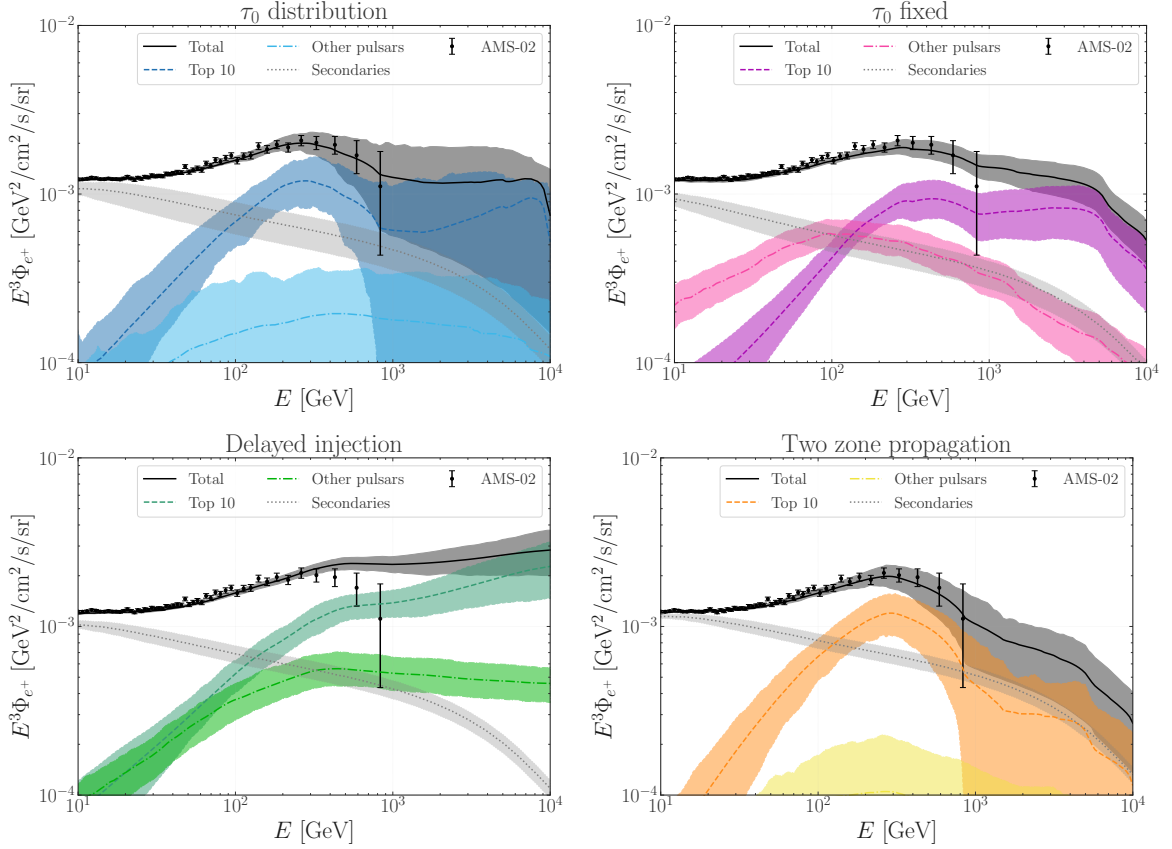


Figure 3: Average values of the fluxes of the top 10 brightest pulsars for each realization that successfully fit the AMS-02 e^+ data, of the secondary flux, of the total flux, and of the contributions from other pulsars, along with the 68% containment band, for the 4 different models.

γ_L distribution, except in the model with a fixed τ_0 , which slightly favors smaller γ_L values. This model, with its adoption of a fixed and relatively large τ_0 , tends to produce a fairly flat $E^3\Phi(E)$ across all energies. To account for the rise of e^+ flux in the excess region, a hard spectrum before the break and a steep one afterward are required, allowing $E^3\Phi(E)$ to rise for energies up to 300 GeV and then decrease for higher ones to match the data. Finally, the distribution of E_b reflects the uniform sampling applied initially, with no clear trend emerging.

The 10^{-4} criterion serves also as a filter to highlight pulsars that consistently satisfy this condition across different models, allowing to establish a hierarchy of sources. In Table 3, left block, we report the names of the top 10 pulsars that satisfy more frequently the 10^{-4} criterion (always for the realizations that fits well the data), for all the different setups. In the right block we report the overall top 10 pulsars, determined by combining the frequency of occurrence across all models and averaging by the number of realizations that fit the data for each model, together with their distance, age and spin-down energy. The bold text style refers to the top 10 pulsars from the overall frequency study.

In Fig. 2 (right panel), the average flux percentage produced by the top 10 brightest sources listed in column 5, Table 3, is shown along with the 68% containment band for the different models, normalized to the total flux produced by all the pulsars. With respect to

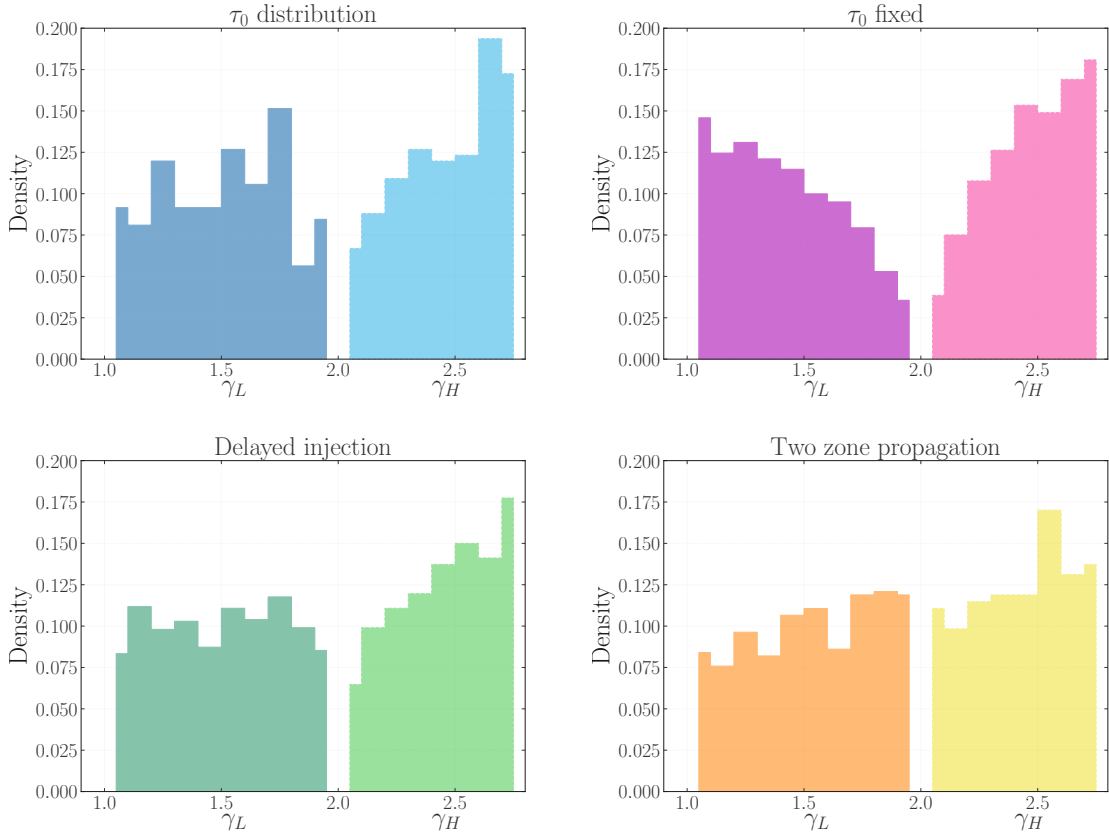


Figure 4: Distribution of the emission spectrum parameters for the brightest sources as selected from the realizations that successfully fit AMS-02 e^+ data for the four setups investigated: τ_0 distribution (upper left), τ_0 fixed (upper right), delayed injection (lower left), two zone propagation (lower right). In each panel, the histograms (normalized to the total number of selected realizations) of the two injection spectral parameters γ_L and γ_H as defined in Eq.(2.1) are reported.

the left panel of Fig. 2, for **τ_0 distribution** there is a larger uncertainty band, both due to the lower number of realizations that fit the data and to the high statistical variance that can promote one random source to be extremely bright when τ_0 occurs to be small. The results for **τ_0 fixed** and **Delayed injection**, namely the models that smooth the most the statistical fluctuations, are similar to the left panel. In the **Two zone** model, the e^+ excess energy range is almost completely dominated by B1055-52, as we will discuss later. The location of this source close to the Earth, and its low diffusion bubble make its contribution dominant with respect to all the other sources.

The translation of the percentage reported in Fig. 2 (right panel) into a flux is reported in Fig. 5. Considering the uncertainties, the top 10 overall sources produce a major contribution to the e^+ flux independently of the model.

In Fig. 6 the average percentage contribution from the top 10 brightest sources among the different models at 200 GeV is shown along with the 68% containment band. A clear hierarchy emerges, with B1055-52 and J0633+1746 (Geminga) playing a significant role across all models. B0656+14 (Monogem), although frequently satisfying the 10^{-4} criterion, contributes

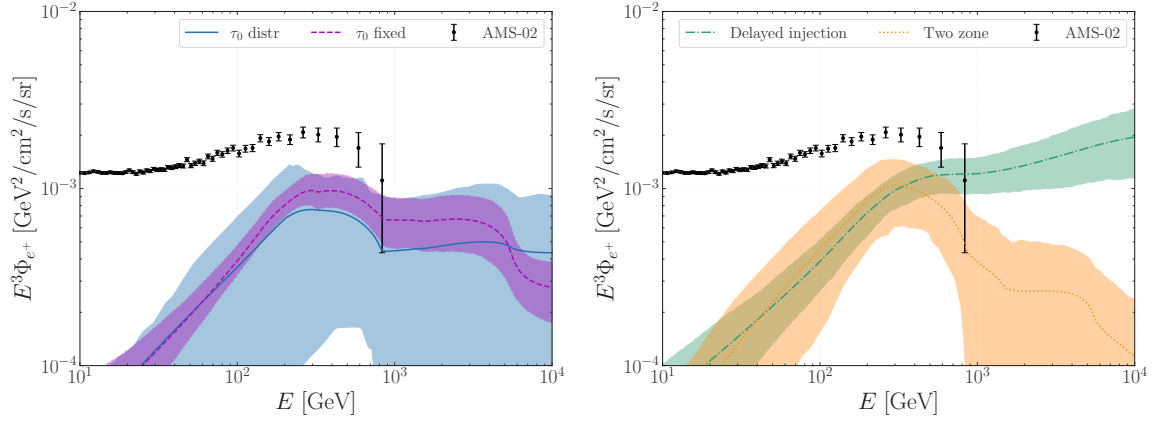


Figure 5: Flux of the top 10 overall sources identified with the 10^{-4} criterion and reported in column 5 of Table 3.

τ_0 distribution	τ_0 fixed	Delayed injection	Two zone	Overall	d [kpc]	t [kyr]	\dot{E} [erg/s]
B1055-52	B1055-52	B1055-52	B1055-52	B1055-52	0.093	535.0	3×10^{34}
J0633+1746	J1732-3131	J0633+1746	J0633+1746	J0633+1746	0.19	342.0	3.2×10^{34}
B0656+14	J0633+1746	B1742-30	B1742-30	B0656+14	0.288	111.0	3.8×10^{34}
B0355+54	J2043+2740	B0656+14	B1738-08	J1732-3131	0.64	111.0	1.5×10^{35}
J1732-3131	B0906-49	J2043+2740	B1749-28	B0355+54	1.0	564.0	4.5×10^{34}
J2030+4415	B0656+14	B1738-08	J0957-5432	J2043+2740	1.48	1200.0	5.6×10^{34}
B0743-53	B0355+54	J1732-3131	J2030+4415	B1742-30	0.2	546.0	8.5×10^{33}
J1020-5921	J0538+2817	J0954-5430	B0743-53	J2030+4415	0.72	555.0	2.2×10^{34}
J0954-5430	J2030+4415	J2030+4415	J0945-4833	B0906-49	1.0	112.0	4.9×10^{35}
B1742-30	J1016-5819	B0355+54	B1001-47	J0538+2817	1.3	618.0	4.9×10^{34}

Table 3: Left block: list of the top 10 pulsars names that satisfy more frequently the 10^{-4} criterion, for each simulation setup. Right block: the top 10 pulsars determined by combining the frequency of occurrence across all models and averaging by the number of realizations that fit the data for each model, together with their distance, age and spin-down energy. The bold text style refers to the top 10 pulsars in column 5.

more at higher energies due to its younger age, and is less dominant at 200 GeV.

From Table 3, it is clear how the e^+ brightest sources are largely consistent across the different models, except for **Two zone**, which is mainly dominated by B1055-52. From the characteristics listed in Table 3, it becomes clear that the dominant sources share some key factors: a distance of less than 1 kpc, an age under 600 kyr, and a spin-down power of more than 10^{34} erg/s. The leading sources meet all three criteria, highlighting how the dominance is primarily determined by age, distance, and energy output.

In Fig. 7 the average fluxes obtained from the realizations that fit well the data are reported, with the 68% containment band, for the three sources of the top 10 overall ranking, B1055-52, J0633+1746 (Geminga) and B0656+14 (Monogem), for all the tested models. For Geminga it is possible to directly compare the predicted flux obtained with the **Two zone** model with the results shown in [16], where the flux from this source was constrained by the results found with a multi-wavelength analysis performed on the Geminga pulsar halo. The flux in [16] turned out to be higher with respect to our prediction, but it was obtained with different spectral index of the injection spectrum of the pulsar, and a different size of the bubble. Those results are still compatible with our new prediction within the uncertainty

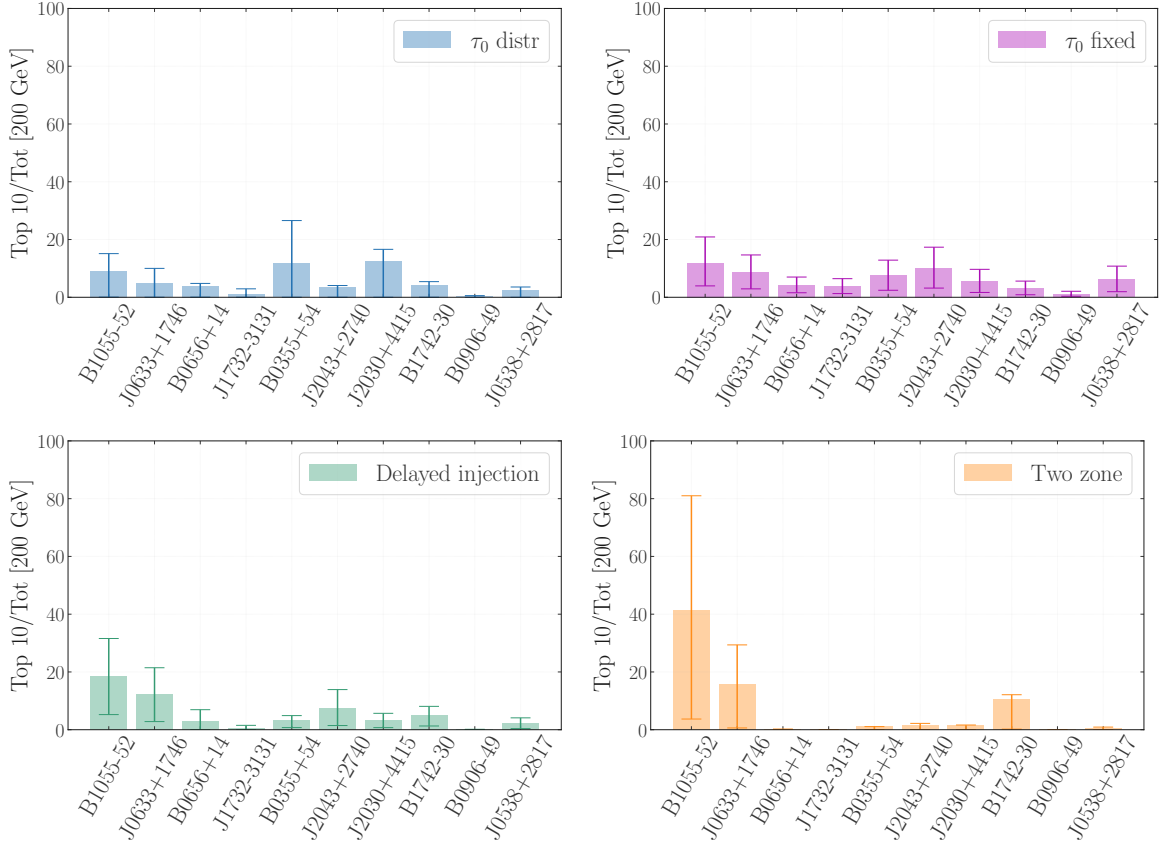


Figure 6: Here are reported the average percentage contributions, together with the 68% containment bands, from the top 10 brightest sources among the different models at 200 GeV listed in column 5 of Table 3.

band. Fig. 7 shows how the flux coming from these "three musketeers" produces a high contribution in all the four setups, with B1055-52 producing an almost dominant flux within the **Two zone** model.

3.3 The anisotropy of the e^+ flux

The anisotropy of the e^+ flux could in principle be a valid complementary observable in order to understand some physical properties of the emitting sources [35]. We show in Fig. 8 the results of the total e^+ dipole anisotropy resulting from the contribution of all sources for the realizations that produce a good fit to the data for **τ_0 distribution**, **τ_0 fixed** and **Delayed injection** models. We compute the anisotropy for each realization, and provide the average value together with the 68% containment band. We predict an anisotropy level between 10^{-4} and 10^{-3} in the whole energy range. **τ_0 distribution**, which is the model that more frequently present the domination of a few pulsars, produce a higher anisotropy level with respect to the others, but still well below the AMS-02 upper limits of Δ_{e^+} obtained from the 10 years data [94], which stand at least two orders of magnitude above our predictions. It is therefore evident that the properties of ATNF pulsars as emerging from AMS-02 flux data are very unlikely be tested by present or forthcoming data on the e^+ anisotropy. Our

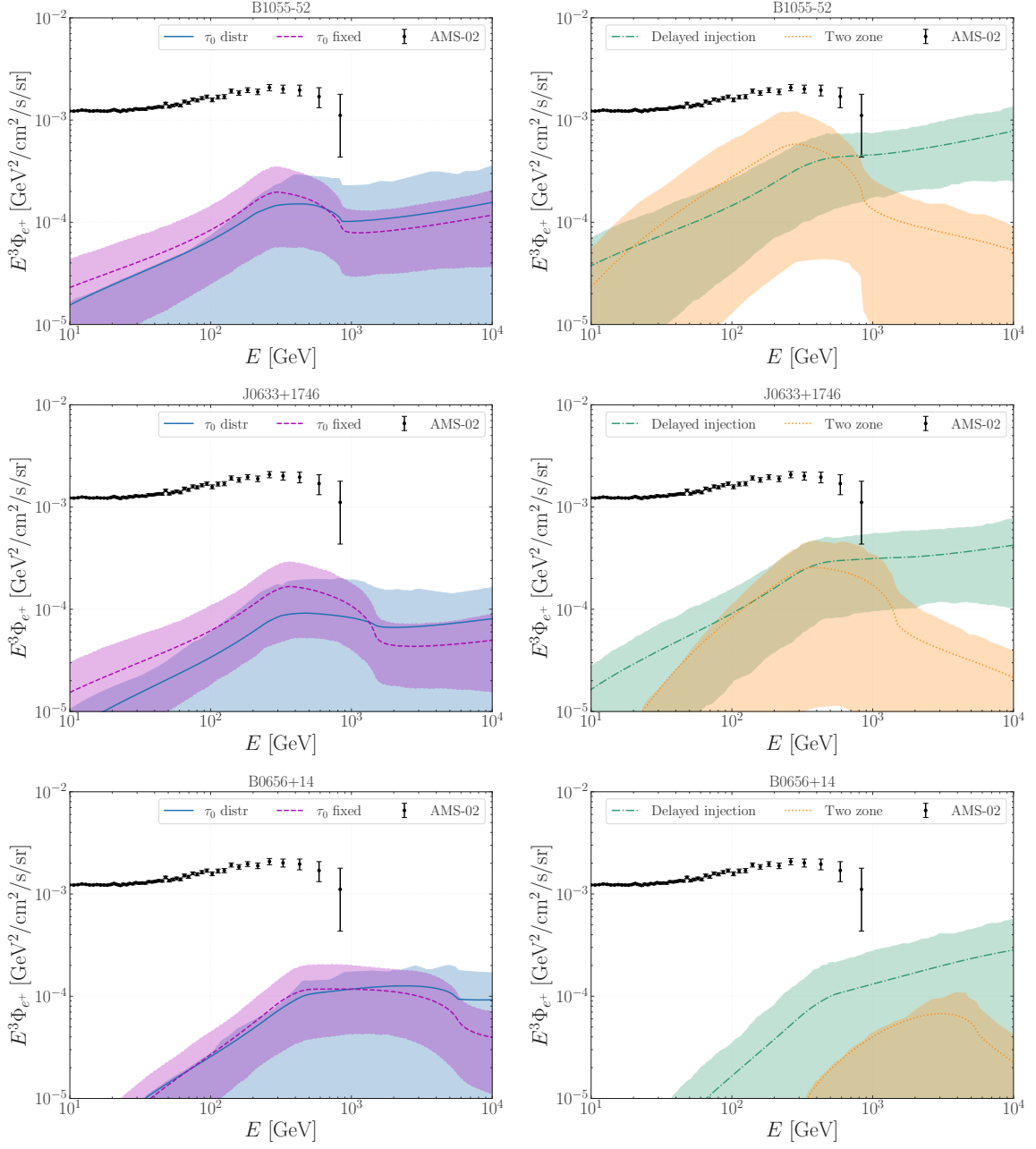


Figure 7: Average fluxes obtained from the realizations that fit well the data, with the 68% containment band, for the three sources of the top 10 overall ranking, B1055-52, J0633+1746 (Geminga) and B0656+14 (Monogem), for all the tested model.

results are similar to the ones found in [35], but with an updated comparison to available experimental upper limits, and using model tuned to the recent insights on e^\pm emission coming from multi-wavelength observations.

4 Status and perspectives of multi-wavelength insights for the most relevant sources

These top 10 sources listed in column 5 of Table 3 are identified as candidates that could significantly contribute to the e^+ flux at Earth across all setups in our investigations of catalog pulsars. We provide here a summary of their main multi-wavelength observations, focusing on those that could help more to constrain the properties of the injected e^\pm .

4.1 The "three musketeers"

The first three spots of the list provided in column 5 of Table 3 are occupied by the three middle-aged pulsars B1055-52, B0656+14, and J0633+1746, that share similar spin-down properties and have been dubbed the 'three musketeers' due to their bright, soft X-ray and high-energy γ -ray emissions [95].

According to the latest version of the ATNF catalog, the pulsar B1055-52 (J1057-5226) is located at a distance of 0.093 kpc. However, the true distance to B1055-52 remains uncertain, varying between 714 and 93 pc depending on the Galactic free-electron density models used: [44] and [43], respectively, despite both using the same dispersion measure. This pulsar is highly energetic, with a spin-down power of 3×10^{34} erg/s and a spin-down age of 535 kyr. Even if a distance of 714 pc is considered, which would reduce the expected e^+ flux, the combination of its \dot{E} and t values suggests that B1055-52 would likely still rank among the top 10 most significant sources when compared to the characteristics of the other leading pulsars reported in Table 3. Alongside Geminga and Monogem, B1055-52 is one of the most studied nearby middle-aged pulsars, showing γ -ray, X-ray, and radio emissions, as highlighted in a recent multi-wavelength study [96]. The pulsar is associated with the point-like γ -ray source 4FGL J1057.9-5227 in the Fermi-LAT 4FGL catalog [97], showing emissions up to a few GeV. No TeV emissions have been detected thus far. A significant X-ray flux has been observed, including in the recent eRASS:4 catalog obtained by SRG/eROSITA in the 0.2-2.3 keV energy band [98]. Although prominent PWN emission has not been detected in the X-ray band, faint extended emission in a small annulus around the pulsar, possibly linked to its PWN, has been observed by Chandra [99]. The possible detection of a γ -ray halo around this pulsar is very challenging with GeV data from Fermi-LAT because, due to the proximity of the source, the halo could span several tens of degrees or even cover the entire sky. Detecting a signal in X-ray data is also likely prohibitive due to the typically small field of view of detectors. However, at multi-TeV energies, this source can be detected as an extended source a few degrees in size. It is not within the field of view of HAWC or LHAASO, but it can be detected by HESS.

Geminga is a middle-aged pulsar located at a distance of 0.19 kpc, with an age of 342 kyr and a spin-down power of 3.2×10^{34} erg/s. A γ -ray halo has been detected around Geminga at multi-TeV energies by MILAGRO [10], HAWC [11], and HESS [13], as well as at tens of GeV with Fermi-LAT data [16]. Despite efforts to detect a synchrotron halo in the X-ray band using XMM, Chandra, and Nustar [21, 23], and SRG/eRosita [22], no such emission has been found, with an estimated magnetic field strength of the local ISM of sub- μ G. However, these attempts have limitations, such as narrow energy and spatial coverage [21] and short exposure times (400 s) [22]. Previous studies suggest that Geminga could contribute significantly to the e^+ flux, potentially accounting for a few tens of percent of the e^+ flux [16, 100, 101], which is consistent with the contribution estimated in this work. One of the main theoretical

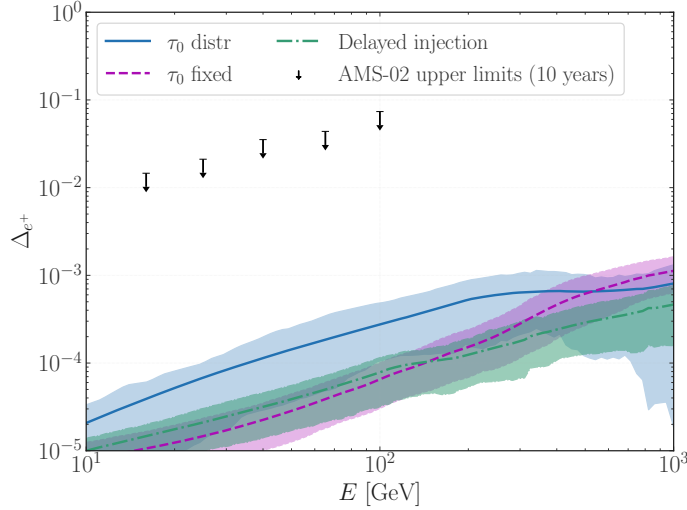


Figure 8: Dipole anisotropy for the realizations that produce a good fit to the data for **τ_0 distribution**, **τ_0 fixed** and **Delayed injection**. We compute the anisotropy for each realization, and we provide the average value together with the 68% containment band. We also show the AMS-02 upper limits of Δ_{e^+} obtained from the 10 years data.

uncertainties is related to the size of the halo where the inhibited diffusion takes place. To narrow down these uncertainties, a future study of Fermi-LAT data is needed, where the halo size is estimated alongside the pulsar efficiency and diffusion coefficient.

Monogem is another well-studied, nearby middle-aged pulsar, located at a distance of 0.288 kpc with a spin-down age of 111 kyr and a spin-down power of 3.8×10^{34} erg/s. Discovered as a radio pulsar, it exhibits thermal and non-thermal emission across multiple wavelengths, from radio to γ rays [102–104]. The properties of the pulsar are consistent with those of the Monogem Ring supernova remnant, an expansive X-ray structure spanning about 25 degrees. An X-ray PWN was identified around the pulsar, with a radius between 0.005 and 0.2 pc, using Chandra data [105]. This pulsar is younger than Geminga, so it produces, on average, more energetic e^\pm . As a consequence, its contribution to the e^+ flux is expected to be at the higher end of the observed data. Moreover, the detection of the γ -ray halo in Fermi-LAT data is challenging due to its angular proximity to Geminga, which is much brighter at GeV energies.

Alongside Geminga, Monogem was found by HAWC to exhibit a γ -ray halo extending a few degrees at multi-TeV energies [11], although only upper limits were obtained when searching for an extended GeV counterpart with Fermi-LAT [16]. Recent multimessenger studies [16, 106, 107] suggest that Monogem contributes only a few percent to the e^+ flux.

The potential significance of the "three musketeers" in explaining the e^+ excess was recently reiterated in [108]. However, their study was limited to a two-zone diffusion scenario and did not account for statistical variation of the injection parameters, nor did it include a fit to the data.

In conclusion, these three pulsars could dominate the contribution to the e^+ flux. To verify this hypothesis, a search for their γ -ray halos is required to estimate the efficiency η , diffusion coefficient D_0 , and the size of the inhibited diffusion region. To achieve this,

large field-of-view MeV and GeV observations with Fermi-LAT, as well as with future γ -ray telescopes should be utilized for the analysis of the Geminga halo. In contrast, a dedicated observational campaign by HAWC and LHAASO is needed for Monogem, while HESS data could give insights on B1055-52.

4.2 Other relevant sources

In this subsection, we continue discussing the multi-wavelength observations of additional relevant sources identified in Section 3.

The pulsar J1732-3131 is a middle-aged pulsar located 0.64 kpc away, with an age of 111 kyr and a current spin-down power of 1.5×10^{35} erg/s. Initially discovered as a radio-quiet γ -ray pulsar, recent intriguing detections at decameter wavelengths have also been reported [109]. This pulsar is positioned near the Galactic center ($l=356.307$, $b=1.007$). There is no firm detection of this source at TeV energies, and it is not listed as an extended source in Fermi-LAT catalogs. Additionally, it falls outside the field of view of HAWC.

The pulsar B0355+54, also known as PSR J0358+5413, is a middle-aged pulsar located at a distance of 1 kpc, with an age of 564 kyr and a spin-down power of 4.5×10^{34} erg/s. In the TeVcat catalog, there is an entry for a nearby 3HWC source, but this is associated with another pulsar, PSR J0359+5414, which has a significantly larger spin-down power and is slightly younger². Additionally, in the first LHAASO catalog [110], the source 1LHAASO J0359+5406 is located very close to B0355+54, but its association remains unclear, as it may also be related to PSR J0359+5414.

J2043+2740 is a very old pulsar, with an age of 1200 kyr, that has been well-characterized in γ rays [111]. Pulsations from this source have also been detected in radio. Despite being one of the oldest non-recycled pulsars observed in γ rays, it remains notably bright with a spin-down power of 5.6×10^{34} erg/s, making it a valuable source for constraining magnetosphere models. The ATNF catalog lists its distance as 1.48 kpc. There are no nearby objects associated with it in TeV catalogs, nor is there evidence of nebular emission in X-rays. However, J2043+2740 is X-ray bright and is among the few old, non-recycled, rotation-powered pulsars detected in X-rays [112].

The pulsar B1742-30, also known as J1745-3040 is a close (0.2 kpc) middle-aged (546 kyr) pulsar with spin-down power of $8.5 \cdot 10^{33}$ erg/s. This source has been studied together with Geminga, Monogem and other close sources as possible significant contributor to the observed e^+ flux, see e.g. [3]. Given its sky location close to the Galactic center, the identification of multi-wavelength counterparts is challenging. The pulsar is spatially coincident with a TeV extended source exhibiting a complicated morphology, HESS J1745-303, located close to SNR G359.1-0.5, and thus possibly identified as Supernova Remnant/molecular cloud emission, though a leptonic contribution from e^\pm coming from a high energetic pulsar cannot be excluded [113].

The source J2030+4415 is a 555 kyr γ -ray pulsar located at 0.72 kpc, with a spin-down power of 2.2×10^{34} erg/s. It is very bright in GeV γ rays, although no TeV counterpart has been identified so far. Notably, a striking X-ray filament has been observed, which is interpreted as a shock structure where e^\pm are being accelerated to TeV energies [114, 115].

B0906-49 is a pulsar located at a distance of 1 kpc, with an age of 112 kyrs and a current spin-down power of 4.9×10^{35} erg/s. While no TeV counterpart has been identified in TeV

²<http://tevcat.uchicago.edu/?mode=1&showsrc=420>

catalogs, it is listed as a point-like source in the Fermi-LAT catalog. A weak extended radio emission, possibly associated with its PWN, has also been detected [116].

The pulsar J0538+2817 was discovered as radio pulsar, and it is usually associated to the supernova remnant SNR S147. It is located at 1.3 kpc, with a characteristic age of 618 kyr and $\dot{E} = 4.9 \cdot 10^{34}$ erg/s. A faint nebula and pulsation are detected in X-rays [117], and gamma ray, radio, and $H\alpha$ emission regions are spatially correlated with the remnant [118]. Recently, the discovery of a one-sided radio filament within the SNR has been claimed [119], which can be produced by the escape of energetic e^\pm from the pulsar into the surrounding supernova remnant, constituting a possible radio analogue of the filaments observed in X-rays for the Guitar and Lighthouse nebulae.

5 Conclusions

In this paper, we use the high-precision AMS-02 e^+ data to constrain key properties of the Galactic pulsar population required to explain the observed CR e^+ flux. By modeling the emission from pulsars listed in the latest version of the ATNF catalog [42] and fitting their contributions to AMS-02 data [1], we find that a combination of their contribution with the secondary production of e^+ emission can account for the majority of the observed e^+ flux, especially at high energies.

To predict a pulsar’s contribution to the e^+ flux at Earth, we use the pulsar’s characteristics—such as distance, age, and spin-down power—obtained from the ATNF catalog. Particle emission properties, which are not directly measurable for each pulsar, are modeled using state-of-the-art phenomenological models based on current theoretical knowledge and constrained by multi-wavelength observations of pulsars and their surrounding nebulae and halos. In this analysis, we consider different assumptions for the injection spectrum of e^\pm , spin-down and particle transport models.

For each realization, we compute the e^+ flux at Earth as the sum of a primary component due to pulsar emission and a secondary component from the fragmentation of CRs interacting with the ISM. The results are then fitted to AMS-02 e^+ data. We find that a fraction of the realizations provide an excellent fit to AMS-02 data.

The pulsar contribution models we explored consistently show that the e^+ flux is dominated by a small number of nearby, middle-aged pulsars, particularly those within 1 kpc of Earth. Notably, the top 10 brightest pulsars can contribute up to 80% of the total e^+ flux at energies above 100 GeV, reaffirming previous findings that a small number of sources can account for the majority of the e^+ excess [41].

The implications of these findings are twofold: we reinforce the importance of local, high-energy pulsars in explaining the e^+ excess, and we emphasize the need for multi-wavelength follow-up observations of the most important sources listed in this analysis. More precise γ -ray observations of the extended halos around these pulsars, as well as studies of synchrotron emission in the X-ray band, are essential to constrain the injection spectra and e^+ diffusion properties, see e.g. the case of Geminga [23]. We provide a list of the 10 most important sources identified across the different tested models, which should be the primary focus of future multi-wavelength analyses.

Specifically, B1055-52, Geminga (J0633+1746), and Monogem (B0656+14) consistently emerge as the primary contributors across all tested models and stand out as prime targets for future γ -ray observations, particularly with instruments like Fermi-LAT and observatories like HAWC, LHAASO, and HESS, as well as with future TeV observatories like CTA [120],

and SWGO [121]. Regarding X-ray observations, detecting the synchrotron counterpart of the Inverse Compton pulsar halos with current X-ray telescopes is challenging due to the proximity of these sources (< 1 kpc) [23]. However, future wide field-of-view X-ray telescopes, as well as observations targeting more distant Galactic pulsars, could still provide valuable insights into the properties of the emitted e^\pm on a population-wide scale.

These results provide a solid foundation for future observational campaigns focused on these pulsars, which will be key to refining our understanding of cosmic ray e^+ transport and the physical processes governing pulsar emission.

Acknowledgments

We thank H. Hakobyan and S. Recchia for inspiring discussion. LO acknowledges the support of the Multimessenger Plasma Physics Center (MPPC), NSF grants PHY2206607. SM acknowledges the European Union’s Horizon Europe research and innovation program for support under the Marie Skłodowska-Curie Action HE MSCA PF-2021, grant agreement No.10106280, project *VerSi*. The work of FD is supported by the Research grant *The Dark Universe: A Synergic Multimessenger Approach*, No. 2017X7X85K funded by the MIUR. FD and MDM acknowledge support from the research grant *TAsP (Theoretical Astroparticle Physics)* funded by Istituto Nazionale di Fisica Nucleare (INFN).

References

- [1] AMS COLLABORATION collaboration, *Towards understanding the origin of cosmic-ray positrons*, *Phys. Rev. Lett.* **122** (2019) 041102.
- [2] T. Delahaye, F. Donato, N. Fornengo, J. Lavalle, R. Lineros, P. Salati et al., *Galactic secondary positron flux at the Earth*, *Astron. Astrophys.* **501** (2009) 821 [0809.5268].
- [3] M. Boudaud et al., *A new look at the cosmic ray positron fraction*, *Astron. Astrophys.* **575** (2015) A67 [1410.3799].
- [4] M. Di Mauro, F. Donato, N. Fornengo et al., *Interpretation of AMS-02 electrons and positrons data*, *JCAP* **1404** (2014) 006 [1402.0321].
- [5] C. Evoli, E. Amato, P. Blasi and R. Aloisio, *Galactic factories of cosmic-ray electrons and positrons*, *Phys. Rev. D* **103** (2021) 083010 [2010.11955].
- [6] M. Di Mauro, F. Donato, M. Korsmeier, S. Manconi and L. Orusa, *Novel prediction for secondary positrons and electrons in the galaxy*, *Physical Review D* **108** (2023) .
- [7] L. Orusa, M. Di Mauro, F. Donato and M. Korsmeier, *New determination of the production cross section for secondary positrons and electrons in the galaxy*, *Physical Review D* **105** (2022) .
- [8] A.M. Bykov, E. Amato, A.E. Petrov, A.M. Krassilchtchikov and K.P. Levenfish, *Pulsar wind nebulae with bow shocks: non-thermal radiation and cosmic ray leptons*, *Space Sci. Rev.* **207** (2017) 235 [1705.00950].
- [9] E. Amato, *The theory of Pulsar Wind Nebulae: recent progress*, *PoS HEPROVII* (2020) 033 [2001.04442].
- [10] A.A. Abdo, B.T. Allen, T. Aune et al., *Milagro Observations of Multi-TeV Emission from Galactic Sources in the Fermi Bright Source List*, *ApJL* **700** (2009) L127 [0904.1018].
- [11] HAWC collaboration, *Extended gamma-ray sources around pulsars constrain the origin of the positron flux at Earth*, *Science* **358** (2017) 911 [1711.06223].

- [12] A. Albert, R. Alfaro, J.C. Arteaga-Velázquez, H.A. Ayala Solares, E. Belmont-Moreno, T. Capistrán et al., *HAWC Detection of a TeV Halo Candidate Surrounding a Radio-quiet Pulsar*, *ApJL* **944** (2023) L29 [[2301.04646](#)].
- [13] H.E.S.S. collaboration, *Detection of extended gamma-ray emission around the Geminga pulsar with H.E.S.S.*, *Astron. Astrophys.* **673** (2023) A148 [[2304.02631](#)].
- [14] F. Aharonian, Q. An, L.X. Axikegu, Bai, Y.X. Bai, Y.W. Bao, D. Bastieri et al., *Extended Very-High-Energy Gamma-Ray Emission Surrounding PSR J 0622 +3749 Observed by LHAASO-KM2A*, *Phy. Rev. Lett.* **126** (2021) 241103 [[2106.09396](#)].
- [15] Z. Cao et al., *Lhaaso detection of very-high-energy gamma-ray emission surrounding psr j0248+6021*, [2410.04425](#).
- [16] M. Di Mauro, S. Manconi and F. Donato, *Detection of a γ -ray halo around Geminga with the Fermi -LAT data and implications for the positron flux*, *Phys. Rev. D* **100** (2019) 123015 [[1903.05647](#)].
- [17] T. Linden, K. Auchettl, J. Bramante, I. Cholis, K. Fang, D. Hooper et al., *Using HAWC to discover invisible pulsars*, *Phys. Rev.* **D96** (2017) 103016 [[1703.09704](#)].
- [18] M. Di Mauro, S. Manconi and F. Donato, *Evidences of low-diffusion bubbles around Galactic pulsars*, *Phys. Rev. D* **101** (2020) 103035 [[1908.03216](#)].
- [19] M. Di Mauro, S. Manconi, M. Negro and F. Donato, *Investigating γ -ray halos around three HAWC bright sources in Fermi-LAT data*, [2012.05932](#).
- [20] D. Hooper and T. Linden, *Evidence of TeV halos around millisecond pulsars*, *Phys. Rev. D* **105** (2022) 103013 [[2104.00014](#)].
- [21] R.-Y. Liu, C. Ge, X.-N. Sun and X.-Y. Wang, *Constraining the Magnetic Field in the TeV Halo of Geminga with X-Ray Observations*, *Astrophys. J.* **875** (2019) 149 [[1904.11438](#)].
- [22] A. Khokhriakova, W. Becker, G. Ponti, M. Sasaki, B. Li and R.Y. Liu, *Searching for X-Ray Counterparts of Degree Wide TeV Halos Around Middle-Aged Pulsars with SRG/eROSITA*, [2310.10454](#).
- [23] S. Manconi, J. Woo, R.-Y. Shang, R. Krivonos, C. Tang, M. Di Mauro et al., *Geminga's pulsar halo: an X-ray view*, *Astron. Astrophys.* **689** (2024) A326 [[2403.10902](#)].
- [24] B.M. Gaensler, N.S. Schulz, V.M. Kaspi, M.J. Pivovarov and W.E. Becker, *XMM-Newton Observations of PSR b1823-13: An asymmetric synchrotron nebula around a vela-like pulsar*, *The Astrophysical Journal* **588** (2003) 441.
- [25] P. Slane, *Pulsar Wind Nebulae, Handbook of Supernovae*, ISBN 978-3-319-21845-8. Springer International Publishing AG, 2017, p. 2159, [1703.09311](#).
- [26] C. Evoli, T. Linden and G. Morlino, *Self-generated cosmic-ray confinement in TeV halos: Implications for TeV γ -ray emission and the positron excess*, *Phys. Rev.* **D98** (2018) 063017 [[1807.09263](#)].
- [27] R. López-Coto and G. Giacinti, *Constraining the properties of the magnetic turbulence in the Geminga region using HAWC γ -ray data*, *Mon. Not. Roy. Astron. Soc.* **479** (2018) 4526 [[1712.04373](#)].
- [28] R.-Y. Liu, H. Yan and H. Zhang, *Understanding the Multiwavelength Observation of Geminga's TeV Halo: The Role of Anisotropic Diffusion of Particles*, *Phys. Rev. Lett.* **123** (2019) 221103 [[1904.11536](#)].
- [29] K. Fang, X.-J. Bi and P.-F. Yin, *Possible origin of the slow-diffusion region around Geminga*, *Mon. Not. Roy. Astron. Soc.* **488** (2019) 4074 [[1903.06421](#)].
- [30] S. Recchia, M. Di Mauro, F. Aharonian, L. Orusa, F. Donato, S. Gabici et al. *Physical Review D* **104** (2021) .

- [31] P. Mukhopadhyay and T. Linden, *Self-generated cosmic-ray turbulence can explain the morphology of tev halos*, *Phys. Rev. D* **105** (2022) 123008.
- [32] E. Amato and S. Recchia, *Gamma-ray halos around pulsars: impact on pulsar wind physics and galactic cosmic ray transport*, *Riv. Nuovo Cim.* **47** (2024) 399 [2409.00659].
- [33] D. Malyshev, I. Cholis and J. Gelfand, *Pulsars versus Dark Matter Interpretation of ATIC/PAMELA*, *Phys. Rev.* **D80** (2009) 063005 [0903.1310].
- [34] M. Di Mauro, F. Donato, N. Fornengo, R. Lineros and A. Vittino, *Interpretation of AMS-02 electrons and positrons data*, *JCAP* **4** (2014) 6 [1402.0321].
- [35] S. Manconi, M. Di Mauro and F. Donato, *Dipole anisotropy in cosmic electrons and positrons: inspection on local sources*, *JCAP* **01** (2017) 006 [1611.06237].
- [36] O. Fornieri, D. Gaggero and D. Grasso, *Features in cosmic-ray lepton data unveil the properties of nearby cosmic accelerators*, *Journal of Cosmology and Astroparticle Physics* **2020** (2020) 009.
- [37] M. Di Mauro, F. Donato and S. Manconi, *On the interpretation of the latest AMS-02 cosmic ray electron spectrum*, [2010.13825](#).
- [38] I. Cholis, T. Karwal and M. Kamionkowski, *Studying the milky way pulsar population with cosmic-ray leptons*, *Physical Review D* **98** (2018) .
- [39] C. Evoli, E. Amato, P. Blasi and R. Aloisio, *Galactic factories of cosmic-ray electrons and positrons*, *Physical Review D* **103** (2021) .
- [40] S. Manconi, M. Di Mauro and F. Donato, *Contribution of pulsars to cosmic-ray positrons in light of recent observation of inverse-Compton halos*, *Phys. Rev. D* **102** (2020) 023015 [2001.09985].
- [41] L. Orusa, S. Manconi, F. Donato and M. Di Mauro, *Constraining positron emission from pulsar populations with ams-02 data*, *JCAP* **2021** (2021) 014.
- [42] R.N. Manchester, G.B. Hobbs, A. Teoh and M. Hobbs, *The Australia Telescope National Facility pulsar catalogue*, *Astron. J.* **129** (2005) 1993 [astro-ph/0412641].
- [43] J.M. Yao, R.N. Manchester and N. Wang, *A new electron-density model for estimation of pulsar and frb distances*, *The Astrophysical Journal* **835** (2017) 29.
- [44] J.M. Cordes and T.J.W. Lazio, *NE2001. 1. A New model for the galactic distribution of free electrons and its fluctuations*, [astro-ph/0207156](#).
- [45] C. Venter, A. Kopp, A.K. Harding, P.L. Gonthier and I. Buesching, *The millisecond pulsar contribution to the rising positron fraction*, 2015.
- [46] A.U. Abeysekara et al., *The 2HWC HAWC Observatory Gamma Ray Catalog*, *Astrophys. J.* **843** (2017) 40 [1702.02992].
- [47] H. Yuksel, M.D. Kistler and T. Stanev, *TeV Gamma Rays from Geminga and the Origin of the GeV Positron Excess*, *Phys. Rev. Lett.* **103** (2009) 051101 [0810.2784].
- [48] D.F. Torres, A. Cillis, J. Martín and E. de Oña Wilhelmi, *Time-dependent modeling of TeV-detected, young pulsar wind nebulae*, *JHEAp* **1-2** (2014) 31 [1402.5485].
- [49] I. Sushch and B. Hnatyk, *Modelling of the radio emission from the Vela supernova remnant*, *Astron. Astrophys.* **561** (2014) A139 [1312.0777].
- [50] I. Buesching, O.C. de Jager, M.S. Potgieter and C. Venter, *A Cosmic Ray Positron Anisotropy due to Two Middle-Aged, Nearby Pulsars?*, *Astrophys. J.* **678** (2008) L39 [0804.0220].
- [51] J.P. Ridley and D.R. Lorimer, *Isolated pulsar spin evolution on the diagram*, *Monthly Notices of the Royal Astronomical Society* **404** (2010) 1081–1088.

- [52] A. Chakraborty and M. Bagchi, *Understanding the Galactic population of normal pulsars: A leap forward*, [2012.13243](#).
- [53] C. Nigro, C. Deil, R. Zanin, T. Hassan, J. King, J.E. Ruiz et al., *Towards open and reproducible multi-instrument analysis in gamma-ray astronomy*, [*Astronomy and Astrophysics* **625** \(2019\) A10](#).
- [54] CTA CONSORTIUM collaboration, *Gammapy - A prototype for the CTA science tools*, [*PoS ICRC2017* \(2018\) 766 \[1709.01751\]](#).
- [55] B.M. Gaensler and P.O. Slane, *The evolution and structure of pulsar wind nebulae*, [*Ann. Rev. Astron. Astrophys.* **44** \(2006\) 17 \[astro-ph/0601081\]](#).
- [56] P. Blasi and E. Amato, *Positrons from pulsar winds*, *Astrophysics and Space Science Proceedings* **21** (2011) 624 [[1007.4745](#)].
- [57] E. van der Swaluw, A. Achterberg, Y.A. Gallant, T.P. Downes and R. Keppens, *Interaction of high-velocity pulsars with supernova remnant shells*, [*A&A* **397** \(2003\) 913–920](#).
- [58] C.-A. Faucher-Giguere and V.M. Kaspi, *Birth and Evolution of Isolated Radio Pulsars*, [*ApJ* **643** \(2006\) 332 \[astro-ph/0512585\]](#).
- [59] T. Delahaye, J. Laval, R. Lineros, F. Donato and N. Fornengo, *Galactic electrons and positrons at the Earth: new estimate of the primary and secondary fluxes*, [*A&A* **524** \(2010\) A51 \[1002.1910\]](#).
- [60] S. Manconi, M. Di Mauro and F. Donato, *Multi-messenger constraints to the local emission of cosmic-ray electrons*, [*JCAP* **04** \(2019\) 024 \[1803.01009\]](#).
- [61] AMS collaboration, *The Alpha Magnetic Spectrometer (AMS) on the international space station: Part II — Results from the first seven years*, [*Phys. Rept.* **894** \(2021\) 1](#).
- [62] E.C. Stone, A.C. Cummings, F.B. McDonald, B.C. Heikkila, N. Lal and W.R. Webber, *Voyager 1 observes low-energy galactic cosmic rays in a region depleted of heliospheric ions*, [*Science* **341** \(2013\) 150 \[https://www.science.org/doi/pdf/10.1126/science.1236408\]](#).
- [63] S. Recchia, S. Gabici, F. Aharonian and J. Vink, *Local fading accelerator and the origin of tev cosmic ray electrons*, [*Physical Review D* **99** \(2019\) .](#)
- [64] R. Cowsik and M.A. Lee, *On the sources of cosmic ray electrons.*, [*ApJ* **228** \(1979\) 297](#).
- [65] S. Vernetto and P. Lipari, *Absorption of very high energy gamma rays in the Milky Way*, [*Phys. Rev.* **D94** \(2016\) 063009 \[1608.01587\]](#).
- [66] LHAASO collaboration, *Extended Very-High-Energy Gamma-Ray Emission Surrounding PSR J0622+3749 Observed by LHAASO-KM2A*, [*Phys. Rev. Lett.* **126** \(2021\) 241103 \[2106.09396\]](#).
- [67] R. Kappl, A. Reinert and M.W. Winkler, *AMS-02 Antiprotons Reloaded*, [*JCAP* **1510** \(2015\) 034 \[1506.04145\]](#).
- [68] Y. Genolini, A. Putze, P. Salati and P. Serpico, *Theoretical uncertainties in extracting cosmic-ray diffusion parameters: the boron-to-carbon ratio*, [*Astron. Astrophys.* **580** \(2015\) A9 \[1504.03134\]](#).
- [69] Y. Génolini et al., *Cosmic-ray transport from AMS-02 boron to carbon ratio data: Benchmark models and interpretation*, [*Phys. Rev. D* **99** \(2019\) 123028 \[1904.08917\]](#).
- [70] S. Profumo, J. Reynoso-Cordova, N. Kaaz and M. Silverman, *Lessons from hawc pulsar wind nebulae observations: The diffusion constant is not a constant; pulsars remain the likeliest sources of the anomalous positron fraction; cosmic rays are trapped for long periods of time in pockets of inefficient diffusion*, [*Physical Review D* **97** \(2018\) .](#)
- [71] X. Tang and T. Piran, *Positron flux and γ -ray emission from Geminga pulsar and pulsar wind nebula*, [*Mon. Not. Roy. Astron. Soc.* **484** \(2019\) 3491 \[1808.02445\]](#).

- [72] S.M. Osipov, A.M. Bykov, A.E. Petrov and V.I. Romansky, *Energetic positron propagation from pulsars: an analytical two-zone diffusion model*, *Journal of Physics: Conference Series* **1697** (2020) 012009.
- [73] C. Evoli, T. Linden and G. Morlino, *Self-generated cosmic-ray confinement in TeV halos: Implications for TeV γ -ray emission and the positron excess*, *Physical Review D* **98** (2018) 063017 [[1807.09263](#)].
- [74] K. Fang, X.-J. Bi and P.-F. Yin, *Possible origin of the slow-diffusion region around Geminga*, *Monthly Notices of the Royal Astronomical Society* **488** (2019) 4074 [[1903.06421](#)].
- [75] P. Mukhopadhyay and T. Linden, *Self-generated cosmic-ray turbulence can explain the morphology of TeV halos*, *Physical Review D* **105** (2022) 123008.
- [76] S. Gupta, D. Caprioli and C.C. Haggerty, *Lepton-driven Nonresonant Streaming Instability*, *The Astrophysical Journal* **923** (2021) 208 [[2106.07672](#)].
- [77] B. Schroer, O. Pezzi, D. Caprioli, C.C. Haggerty and P. Blasi, *Cosmic-ray generated bubbles around their sources*, *Monthly Notices of the Royal Astronomical Society* **512** (2022) 233 [[2202.05814](#)].
- [78] I. Plotnikov, A.J. van Marle, C. Guépin, A. Marcowith and P. Martin, *Kinetic simulations of electron-positron induced streaming instability in the context of gamma-ray halos around pulsars*, *Astronomy and Astrophysics* **688** (2024) A134.
- [79] B. Schroer, C. Evoli and P. Blasi, *TeV halos and the role of pulsar wind nebulae as sources of cosmic-ray positrons*, *Physical Review D* **107** (2023) .
- [80] V. Gingburg and S. Syvoratskii, *The Origin of Cosmic Rays*, Pergamon (1964), <https://doi.org/10.1016/B978-0-08-013526-7.50005-0>.
- [81] C.S. Shen and C.Y. Mao, *Anisotropy of High Energy Cosmic-Ray Electrons in the Discrete Source Model*, *ApJL* **9** (1971) 169.
- [82] F. Donato, D. Maurin and R. Taillet, *Beta-radioactive cosmic rays in a diffusion model: Test for a local bubble?*, *Astronomy and Astrophysics* **381** (2002) 539–559.
- [83] G. Giacinti, M. KachelrieSS and D. Semikoz, *Reconciling cosmic ray diffusion with galactic magnetic field models*, *Journal of Cosmology and Astroparticle Physics* **2018** (2018) 051–051.
- [84] M.C. Beck, A.M. Beck, R. Beck, K. Dolag, A.W. Strong and P. Nielaba, *New constraints on modelling the random magnetic field of the mw*, *Journal of Cosmology and Astroparticle Physics* **2016** (2016) 056–056.
- [85] R. Jansson and G.R. Farrar, *A new model for the galactic magnetic field*, *The Astrophysical Journal* **757** (2012) 14.
- [86] M. Boudaud, E.F. Bueno, S. Caroff, Y. Genolini, V. Poulin, V. Poireau et al., *The pinching method for Galactic cosmic ray positrons: implications in the light of precision measurements*, *Astron. Astrophys.* **605** (2017) A17 [[1612.03924](#)].
- [87] I. Cholis and T. Hoover, *Observing signals of spectral features in the cosmic-ray positrons and electrons from Milky Way pulsars*, *Phys. Rev. D* **107** (2023) 063003 [[2211.15709](#)].
- [88] O. Kargaltsev, G.G. Pavlov, C. Bassa, Z. Wang, A. Cumming and V.M. Kaspi, *Pulsar wind nebulae in the chandra era*, in *AIP Conference Proceedings*, vol. 983, p. 171–185, AIP, 2008, DOI.
- [89] J.D. Gelfand, P.O. Slane and W. Zhang, *A dynamical model for the evolution of a pulsar wind nebula inside a nonradiative supernova remnant*, *The Astrophysical Journal* **703** (2009) 2051–2067.

- [90] N. Bucciantini, J. Arons and E. Amato, *Modelling spectral evolution of pulsar wind nebulae inside supernova remnants*, *Monthly Notices of the Royal Astronomical Society* **410** (2010) 381 [<https://academic.oup.com/mnras/article-pdf/410/1/381/18446661/mnras0410-0381.pdf>].
- [91] D. Volpi, L. Del Zanna, E. Amato and N. Bucciantini, *Non-thermal emission from relativistic MHD simulations of pulsar wind nebulae: from synchrotron to inverse Compton*, *A&A* **485** (2008) 337 [[0804.1323](#)].
- [92] H. E. S. S. Collaboration, *The exceptionally powerful TeV γ -ray emitters in the Large Magellanic Cloud*, *Science* **347** (2015) 406 [[1501.06578](#)].
- [93] G. Principe, A.M.W. Mitchell, S. Caroff, J.A. Hinton, R.D. Parsons and S. Funk, *Energy dependent morphology of the pulsar wind nebula HESS J1825-137 with Fermi-LAT*, *A&A* **640** (2020) A76 [[2006.11177](#)].
- [94] M. Ángel Velasco, J. Casaus and M. Molero, *Determination of the anisotropy of elementary particles with the alpha magnetic spectrometer on the international space station*, *Advances in Space Research* (2024) .
- [95] W. Becker, N. Kawai, W. Brinkmann and R. Mignani, *The putative pulsar-wind nebulae of the three musketeers psr b1055-52, b0656+14 and geminga revisited*, *Astron. Astrophys.* **352** (1999) 532 [[astro-ph/9910010](#)].
- [96] B. Posselt, G.G. Pavlov, O. Kargaltsev and J. Hare, *X-ray and near-infrared observations of the middle-aged pulsar b1055-52, its multiwavelength spectrum, and proper motion**, *The Astrophysical Journal* **952** (2023) 134.
- [97] S. Abdollahi et al., *Fermi large area telescope fourth source catalog*, *The Astrophysical Journal Supplement Series* **247** (2020) 33.
- [98] M.G.F. Mayer and W. Becker, *Searching for X-ray counterparts of unassociated Fermi-LAT sources and rotation-powered pulsars with SRG/eROSITA*, *Astron. Astrophys.* **684** (2024) A208 [[2401.17295](#)].
- [99] B. Posselt, G. Spence and G.G. Pavlov, *A Chandra Search for the Pulsar Wind Nebula Around psr B1055-52*, *Astrophys. J.* **811** (2015) 96 [[1507.07924](#)].
- [100] D. Hooper, P. Blasi and P.D. Serpico, *Pulsars as the sources of high energy cosmic ray positrons*, *Journal of Cosmology and Astroparticle Physics* **2009** (2009) 025-025.
- [101] D. Hooper, I. Cholis, T. Linden and K. Fang, *HAWC Observations Strongly Favor Pulsar Interpretations of the Cosmic-Ray Positron Excess*, *Phys. Rev. D* **96** (2017) 103013 [[1702.08436](#)].
- [102] M. Durant, O. Kargaltsev and G.G. Pavlov, *Multiwavelength spectroscopy of psr b0656+14*, *The Astrophysical Journal* **743** (2011) 38.
- [103] A. Schwobe et al., *Phase-resolved X-ray spectroscopy of PSR B0656+14 with SRG/eROSITA and XMM-Newton*, *Astron. Astrophys.* **661** (2022) A41 [[2106.14533](#)].
- [104] FERMI-LAT collaboration, *Incremental Fermi Large Area Telescope Fourth Source Catalog*, *Astrophys. J. Supp.* **260** (2022) 53 [[2201.11184](#)].
- [105] L. Bîrzan, G.G. Pavlov and O. Kargaltsev, *Chandra observations of the elusive pulsar wind nebula around psr b0656+14*, *The Astrophysical Journal* **817** (2016) 129.
- [106] Y. Li, O. Macias, S. Ando and J. Vink, *Multi-messenger modeling of the Monogem pulsar halo*, [2406.13426](#).
- [107] P. Martin, A. Marcowith and L. Tibaldo, *Are pulsar halos rare? - Modeling the halos around PSRs J0633+1746 and B0656+14 in the light of Fermi-LAT, HAWC, and AMS-02 observations and extrapolating to other nearby pulsars*, *Astron. Astrophys.* **665** (2022) A132 [[2206.11803](#)].

- [108] K. Fang, X.-J. Bi and P.-F. Yin, *Reanalysis of the pulsar scenario to explain the cosmic positron excess considering the recent developments*, *The Astrophysical Journal* **884** (2019) 124.
- [109] Y. Maan, M.A. Krishnakumar, A.K. Naidu, S. Roy, B.C. Joshi, M. Kerr et al., *Detection of radio emission from the gamma-ray pulsar J1732–3131 at 327 MHz*, *Mon. Not. Roy. Astron. Soc.* **471** (2017) 541 [[1706.08613](#)].
- [110] LHAASO collaboration, *The First LHAASO Catalog of Gamma-Ray Sources*, *Astrophys. J. Suppl.* **271** (2024) 25 [[2305.17030](#)].
- [111] A. Noutsos, A.A. Abdo, M. Ackermann, M. Ajello, J. Ballet, G. Barbiellini et al., *Radio and gamma-ray constraints on the emission geometry and birthplace of psr j2043+2740*, *The Astrophysical Journal* **728** (2011) 77.
- [112] W. Becker, M.C. Weisskopf, A.F. Tennant, A. Jessner, J. Dyks, A.K. Harding et al., *Revealing the x-ray emission processes of old rotation-powered pulsars: XMM-Newton observations of PSR B0950+08, PSR B0823+26 and PSR J2043+2740*, *Astrophys. J.* **615** (2004) 908 [[astro-ph/0405180](#)].
- [113] HESS collaboration, *The H.E.S.S. Galactic plane survey*, *Astron. Astrophys.* **612** (2018) A1 [[1804.02432](#)].
- [114] M. de Vries and R.W. Romani, *The long filament of psr j2030+4415*, *The Astrophysical Journal* **928** (2022) 39.
- [115] M. de Vries and R.W. Romani, *PSR J2030+4415’s Remarkable Bow Shock, PWN, and Filament*, *Astrophys. J. Lett.* **896** (2020) L7 [[2005.13572](#)].
- [116] B.M. Gaensler, B.W. Stappers, D.A. Frail and S. Johnston, *An Unusual pulsar wind nebula associated with PSR B0906-49*, *Astrophys. J. Lett.* **499** (1998) L69 [[astro-ph/9803273](#)].
- [117] R.W. Romani and C.Y. Ng, *The PWN torus of PSR J0538+2817 and the origin of pulsar velocities*, *Astrophys. J. Lett.* **585** (2003) L41 [[astro-ph/0301506](#)].
- [118] X. Tang, *Gamma-ray emission from middle-aged supernova remnants interacting with molecular clouds: the challenge for current models*, *Mon. Not. Roy. Astron. Soc.* **482** (2019) 3843 [[1707.00958](#)].
- [119] I. Khabibullin, E. Churazov, A. Bykov, N. Chugai and I. Zinchenko, *Discovery of a one-sided radio filament of PSR J0538+2817 in S147: escape of relativistic PWN leptons into surrounding supernova remnant?*, *Mon. Not. Roy. Astron. Soc.* **527** (2023) 5683 [[2309.13670](#)].
- [120] CTA CONSORTIUM collaboration, *Introducing the CTA concept*, *Astropart. Phys.* **43** (2013) 3.
- [121] P. Abreu, A. Albert, R. Alfaro, C. Alvarez, R. Arceo, P. Assis et al., *The southern wide-field gamma-ray observatory (swgo): A next-generation ground-based survey instrument for the gamma-ray astronomy*, 2019.